Sampling fractional Brownian motion in presence of absorption: A Markov chain method

Alexander K. Hartmann*
Institute of Physics, University of Oldenburg, Oldenburg, Germany

Satya N. Majumdar and Alberto Rosso
Université Paris-Sud, CNRS, LPTMS, UMR 8626, Orsay F-91405, France

(Received 7 March 2013; revised manuscript received 29 May 2013; published 12 August 2013)

We numerically study fractional Brownian motion (fBm) with an absorbing boundary at the origin for selected values of the Hurst exponent $H \in [0,1]$. Using a Monte Carlo sampling technique, we are able to numerically generate these fBm processes at discrete times for up to 10^7 time steps, even for values as small as $H = 1/4$. The results are compatible with previous analytical results that suggest that the distribution of (rescaled) endpoints y follow a power law $P_+(y) \sim y^\phi$ with $\phi = (1-H)/H$, even for small values of H. Furthermore, for $H = 0.5$ we study analytically the finite-length corrections to first order, namely a plateau of $P_+(y)$ for $y \to 0$ which decreases with increasing process length. These corrections are compatible with our numerical results.

DOI: 10.1103/PhysRevE.88.022119 PACS number(s): 05.40.Fb, 02.50.−r

I. INTRODUCTION

The Brownian motion plays a key role in modern theoretical physics, as it explains many effects observed in physical systems. It is currently used in various fields of science to understand, for instance, the trend of financial markets, the dynamics of complex molecules within cells, and the food-searching strategies of animals. In order to describe the fluctuations in these systems, it is often necessary to go beyond the Brownian motion and consider random walkers whose mean square displacement grows over time in a nonlinear way. The term used to refer to this situation is *anomalous diffusion*, in particular *subdiffusion* if the mean square displacement grows slower than linearly, *superdiffusion* if it is faster.

In practice, anomalous diffusion occurs whenever the process $x(\tau)$ is self-affine (at least at large time) with a characteristic value of the so-called *Hurst exponent* $H \neq 1/2$, so that the displacement grows with time as τ^H. A remarkable example of a process displaying anomalous diffusion is the fractional Brownian motion (fBm) [1]. This process is self-affine Gaussian with $0 < H < 1$. A Gaussian process is completely defined by its autocorrelation function, which for fBm is written as

$$\langle x(\tau)x(\tau')\rangle = \tau^{2H} + (\tau')^{2H} - |\tau - \tau'|^{2H}, \qquad (1)$$

where $x(0) = 0$ and the brackets $\langle \ldots \rangle$ refer to an ensemble average over the realizations of the Gaussian processes. The strength of the correlation is described by the Hurst exponent. Note that Eq. (1) implies $\langle [x(\tau_1) - x(\tau_2)]^2 \rangle = 2|\tau_1 - \tau_2|^{2H}$. This means that $H = 1/2$ corresponds to the Brownian motion (standard diffusion), $H > 1/2$ to superdiffusive paths, and $H < 1/2$ to subdiffusive paths.

Recently these random walks have been found to be relevant for many physical applications. Among them we mention the fluctuations of a tagged monomer of an equilibrated Rouse chain [2,3], or of a tagged particle in the one dimensional system [4,5]. In both cases the motion of the tagged object can be modeled as fractional Brownian motion with $H = 1/4$. Other physical processes such as the mechanical unzipping of DNA [6], the translocation of polymers through nanopores [2,7–9], and subdiffusion of macromolecules inside cells and membranes [10–12] are also well described by fBm diffusion.

Despite the large number of cases where fBm is observed, very little is known about the properties of this process when it is confined to some region of space, which is the case for many of the above mentioned applications. A concrete example is given by polymer translocation. In this case it has been shown [2,7] that the fraction of the polymer penetrated through the nanopore fluctuates with time as a fBm walker confined inside the interval 0 (which corresponds to the translocation failure) and 1 (which corresponds to completed translocation).

In the presence of boundaries, translational invariance is lost and analytical representations such as the fractional Langevin equation are of little help [13]. In these situations, numerical simulations remain the most viable option in answering many concrete questions arising from biology and physics [14–16]. Recently, methods have been developed to study fBm in a system under the influence of a potential [17] and for fBm in confined geometries [18]. Here we present a generic numerical method which we use to study these processes in the presence of boundaries. We study in detail the case where there is an absorbing wall at $x = 0$: we thus consider only the paths that remain positive up to the final time τ. Recently, analytical predictions [7,19] have been obtained for the distribution $P_+(y)$ of rescaled motion endpoints $y \sim x/(\tau^H)$ at end time τ. A possible numerical strategy consists of directly sampling L-step fBm paths $x_0, x_1, \ldots, x_L$ at discrete times, starting at $x_0 = 0$. This strategy is demanding, in particular for $H < 1/2$, since in the presence of an absorbing boundary the success probability of generating a nonabsorbed trajectory is very small. Hence, such simulations were restricted to a small number L of discrete steps. Using a Markov chain approach, we were able to generate long fBm processes up to $L = 10^7$ discrete steps for $H = 1/4$, $2/5$, $1/2$, $2/3$, and $3/4$.

The outline of the remainder of the paper is as follows: Next, we present our numerical approach and then we present our numerical results: In order to verify that our approach is working, we first consider the case of Brownian motion ($H = 1/2$), where analytical results for the finite-length

*a.hartmann@uni-oldenburg.de

corrections are available. We further study the cases $H = 1/4$, $H = 2/5$ and $H = 2/3$, $H = 3/4$ as examples for the two regions $H < 1/2$ and $H > 1/2$. In all cases the results are compatible with previous analytical predictions. Finally, we summarize our results.

II. NUMERICAL METHODS

To generate fBm processes on a computer, we study discrete-time random walks with suitable correlations. It is useful to introduce the increments of the random walk, namely $\Delta x_l = x_{l+1} - x_l$. For Gaussian processes the increments are Gaussian variables defined by their autocorrelation function. Using Eq. (1) we can compute the autocorrelation function of the Gaussian increments:

$$C_{l+m,l} \equiv \langle \Delta x_{l+m} \Delta x_l \rangle = |m+1|^{2H} - 2|m|^{2H} + |m-1|^{2H} \equiv C(m). \quad (2)$$

We note that this function is independent of the initial time l. Matrices having this property are called *Toeplitz matrices*. Moreover, the increments are identically distributed Gaussian numbers with variance $\sigma^2 = 2$ displaying power law correlations. Taking the limit $m \to \infty$, it is easy to extract the power law decay of these correlations. For superdiffusive fBm ($H > 1/2$), $C(m)$ is positively correlated, decaying as $m^{-2(1-H)}$. Positive correlation means that there is a high probability of observing a long sequence of increments of the same sign. For subdiffusive fBm ($H < 1/2$), $C(m)$ is negatively correlated and decays as $-m^{-2(1-H)}$. Negative correlation means that there is a high probability of observing a long sequence of increments of oscillating sign.

The direct generation of L steps with increment correlation Eq. (2) is in principle straightforward. The starting point is a vector $\xi = (\xi_0, \xi_1, \ldots, \xi_{L-1})$ of L independent and identically distributed (iid) Gaussian (mean 0, variance 1) numbers $\sim G(0,1)$. For the uncorrelated case ($H = 1/2$) one could directly use these random numbers, multiplied by $\sqrt{2}$ to obtain the right $C_{l,l}$, as increments of the fBm processes, i.e., $x^{\text{uncorr}}(L) = \sum_{l=0}^{L-1} \sqrt{2}\xi_l$.

For the case $H \neq 1/2$, since C is a positive semidefinite correlation matrix, there exists a matrix A such that $C = A^2$. Thus, one could use $\Delta x = A\xi$ to obtain a random vector satisfying Eq. (2). Nevertheless, this is too time consuming since it requires diagonalizing the $L \times L$ C matrix once ($\sim L^3$ operations) and, for each process, multiplication with the $L \times L$ matrix A ($\sim L^2$ operations) [20]. This is not feasible in practice given the sizes $L = 10^7$ we study here.

Instead, we use the *circulant embedding method* proposed in [21,22] for the fast generation of a Gaussian field. This method allows us to generate random increments which are approximately correlated according to Eq. (2) by generating a periodic increment sequence of period L', with $L' \geqslant 2L$. The correlations of this periodic sequence are encoded in a covariance matrix $\mathcal{C}_{l,l+m} = \mathcal{C}(m)$ of size $L' \times L'$ built using the original covariance C and defined as

$$\begin{aligned} \mathcal{C}(m) &= C(m) \quad \text{for} \quad m = 0, \ldots, L'/2 - 1 \\ \mathcal{C}(m) &= C(L' - m) \quad \text{for} \quad m = L'/2, L' - 1. \end{aligned} \quad (3)$$

Toeplitz matrices displaying this periodicity are called *circulant* matrices. For the analysis of our numerical simulations, we consider only the first L steps $\Delta x_1, \Delta x_2, \ldots, \Delta x_L$. If L is large, the correlation between the first and the last increment is small and the periodicity has no large influence. The advantage of this approach is that the periodicity of the matrix $\mathcal{C}$ allows the application of fast Fourier transformation (FFT) to generate the fBms [23].

The FFT is performed in $\sim L' \log(L')$ operations. We used the GNU Scientific Library (GSL) [24]. Let be $\hat{c}_k$ the FFT of $\mathcal{C}(m)$ from Eq. (3), i.e., $\hat{c}_k = \sum_{m=0}^{L'-1} \mathcal{C}(m) e^{-2\pi i (k/L')m}$. Since $\mathcal{C}(m)$ is symmetric and positive, the coefficients $\hat{c}_k$ are positive real numbers. The generation of the correlated random numbers works as follows:

(i) The starting point is a vector of L' independent and identically distributed (iid) Gaussian numbers (with zero mean and variance 1).

$$\xi = (\xi_0, \xi_1, \ldots, \ldots, \xi_{L-1}).$$

(ii) We define

$$\hat{\delta}_k = \sqrt{L' \hat{c}_k} \xi_k \quad (k = 0, \ldots, L' - 1), \quad (4)$$

which are real numbers as well and where the factor $\sqrt{L'}$ takes into account the correct normalization.

(iii) The vector of increments is obtained after back transforming $\hat{\delta}_k$:

$$\delta_l = \frac{1}{L'} \sum_{k=0}^{L'-1} \hat{\delta}_k e^{2\pi i (l/L')k}, \quad (5)$$

and taking the real and imaginary part:

$$\Delta x_l = \text{Re}\{\delta_l\} + \text{Im}\{\delta_l\} \quad (6)$$

with $l = 1, 2, \ldots, L'$.

It is easy to check that these three steps lead to the desired correlation. Using $\xi_k = \xi_k^*$ and $\langle \xi_k \xi_{k'} \rangle = \delta_{k,k'}$ one arrives at $\langle \delta x_l^{(*)} \delta x_j^{(*)} \rangle = C(\pm i \pm j)$, where the signs are $+$ when δx_l and δx_j on the left, respectively, and $-$ for the conjugate complex. Thus, using $\text{Re}(z) = (z + z^*)/2$, $\text{Im}(z) = (z - z^*)/2i$, and $C(m) = C(-m)$, one obtains

$$\begin{aligned} &\langle \Delta x_{l+m} \Delta x_l \rangle \\ &= \tfrac{1}{4} \langle (\delta_{l+m} + \delta_{l+m}^* - i\delta_{l+m} + i\delta_{l+m}^*)(\delta_l + \delta_l^* - i\delta_l + i\delta_l^*) \rangle \\ &= C(m) \end{aligned}$$

as desired. A numerical test of the method is shown in Fig. 1, which indicates that the randomly generated numbers satisfy Eq. (2).

For direct simulations of fBm processes, one generates a vector of L' random real numbers, constructs the vector of complex numbers ξ, uses the transformation Eqs. (4) and (6) to obtain the correlated increments Δx_l, and then finally

$$x \equiv x(L) = \sum_{l=1}^{L} \Delta x_l. \quad (7)$$

Nevertheless, since we use an absorbing boundary at $x = 0$, most of the time at least one of the intermediate steps will visit the negative half axis, i.e., $\sum_{l=1}^{\ell} \Delta x_l < 0$ (for some $\ell \leqslant L$), in which case the obtained value $x(L)$ does not contribute to

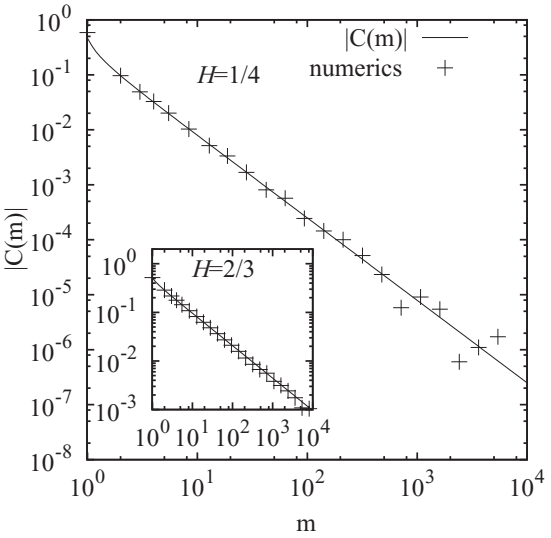

FIG. 1. Correlation between increments. Shown are the desired function $C(m)$ and the numerical data for $L = 10^4$. The main plot is for $H = 1/4$, while the inset displays $H = 2/3$.

the distribution $P_+(y)$. The probability of not being absorbed, i.e., the *persistence* (or survival probability), behaves like

$$S(x_0 = 0, L) \sim L^{-\theta} \tag{8}$$

with θ being the persistence exponent, known to be $\theta = 1 - H$ [3,25,26]. Hence, for the case $L = 10^7$ and $H = 1/4$, we obtain $P_0(L) \approx 10^{-5}$. This means a direct simulation is not feasible. Such an approach has been used in the past [19] for $H \geqslant 1/2$, which is simpler than $H < 1/2$. Moreover, due to the mentioned limitations, even for the simpler case only $L = 20\,000$ could be studied, in contrast to $L = 10^7$, which we study for $H \geqslant 1/2$ as well as $H < 1/2$. Note that an alternative is to directly simulate a physical process which exhibits the nature of fractional Brownian motion, e.g., a suitable polymer model. However, this includes many more physical details than a raw fBm, and hence only even smaller systems can be studied, as for example in a recent study [27] where only polymers with $N = 257$ monomers could be treated.

To circumvent this problem, we performed a Markov chain Monte Carlo simulation with the configuration space consisting of all *feasible* random vectors ξ. Feasible in this context means that the resulting fBm process (after FFT to generate the correlation of the increments Δx) is not absorbed. The simulation must be initialized with an allowed configuration, and therefore we start from a random vector $\xi^{(0)}$ and a corresponding correlated increment $\Delta x^{(0)}$ such that the resulting process is not absorbed. In practice, for $H \leqslant 1/2$, we facilitate the generation of a feasible initial configuration by sampling from a shifted Gaussian $G(\bar{\xi},1)$ ($\bar{\xi} > 0$) and repeat the search for an initial configuration until a feasible increment vector is found. This initial configuration is clearly biased, but does not have influence on the final result since we start to sample the observables only after some sufficient equilibration time.

Each Monte Carlo step $\xi^{(t)} \to \xi^{(t+1)}$ consists of changing a fraction p of randomly chosen entries of the configuration $\xi^{(t)}$, the new entries being iid G(0,1), resulting in a trial configuration ξ^{trial}. Then, again after using FFT to introduce the correlation, we obtain Δx^{trial}: if the resulting fBm $\{\sum_{l=1}^{\hat{L}} \tilde{\Delta} x_l^{\text{trial}}\}$ ($\hat{L} = 1, \ldots, L$) is absorbed, the trial configuration is rejected, i.e., $\xi^{(t+1)} = \xi^{(t)}$. If the resulting fBm is allowed, the trial configuration is feasible and thus is accepted, i.e., $\xi^{(t+1)} = \xi^{\text{trial}}$. This approach satisfies detailed balance, and hence converges to the correct distribution: The distribution of configurations is given by a product of Gaussians over the space of feasible configurations,

$$P(\xi) = \prod_{i=1}^{L'} \left(\frac{1}{\sqrt{2\pi}} \exp\left(-\xi_i^2/2\right) \right) I_\xi,$$

where the indicator function I_ξ is 1 if ξ is feasible (the resulting fBm is not absorbed) and 0 otherwise. Therefore, if a certain fraction p of the entries of ξ is replaced to yield ξ', the resulting change of weight is given by

$$w(\xi \to \xi') = \prod_j{}' \left(\frac{1}{\sqrt{2\pi}} \exp\left(-\xi_j'^2/2\right) \right) I_{\xi'},$$

where the product runs over the altered entries. This change of weight is symmetric with respect to $\xi \leftrightarrow \xi'$, and hence detailed balance is fulfilled: $P(\xi)w(\xi \to \xi') = P(\xi')w(\xi' \to \xi)$.

The Markov chain in the configuration space is reflected by the sequence of endpoints $x^{(0)}(L), x^{(1)}(L), \ldots$ in our Monte Carlo simulation. Here we studied the statistics of the rescaled variable $y = x(L)/(\sigma L^H)$. Since we are interested in the behavior of $P_+(y)$ near $y = 0$, we also used a bias $b(y) = y^{-a}$ ($a > 0$), and imposed the additional Metropolis criterion [28–30] of accepting a feasible configuration with the probability $p_{\text{accept}} = \min\{1, b(y^{\text{trial}})/b(y^{(t)})\}$. This drives the simulation into the range of interest. We adjusted the fraction p of changed entries such that the total acceptance probability of an Monte Carlo (MC) step is near 0.5. Hence, for each value H of the Hurst exponent and each length L, we needed to find a suitable value $p = p(H, L)$ empirically.

In Fig. 2 a sample trajectory in the space of (rescaled) endpoints is shown for $H = 1/2$ and $L = 10^7$. By employing the bias $b(y) \sim y^{-1.2}$, the simulation was concentrated near $y \approx 0$.

Concerning equilibration of our Monte Carlo simulation, we found that typically, for the longer fBm processes, there are no signs of the initial configuration after 1000 sweeps. After disregarding this initial bunch of Monte Carlo sweeps, we measured histograms [31] of the rescaled endpoints of the processes. In the case that a bias is applied, the histograms must be multiplied by $b^{-1} = y^a$ and normalized to get the final distributions $P_+(y)$.

Note that the approach used here is rather general: During the Monte Carlo simulation a vector of variables is changed. This vector, according to a Metropolis criterion is either rejected or accepted. This is like in any Markov chain Monte Carlo simulation, e.g., a single-spin flip simulation of the Ising model. The only difference here is that the step transforming the configuration vector into a Metropolis criterion is rather involved since it includes creating a correlation between the vector entries, turning them into random walks, checking for absorption and including a bias that keeps the random walks close to the origin. For the Ising system the same step

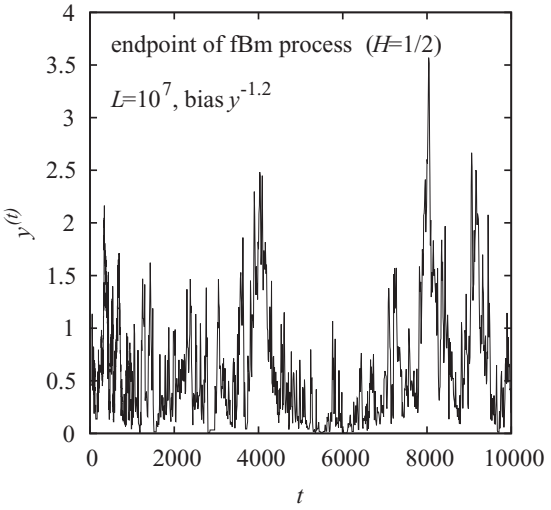

FIG. 2. Sample trajectory of a Monte Carlo simulation: the endpoint $y^{(t)} = x(L)^{(t)}/L^H$ of a nonabsorbed fBm ($H = 1/2$) of length $L = 10^7$ as a function of the MC time t, for the initial phase of the MC simulation up to $t = 10^4$. A bias $\sim y^{-1.2}$ is used to increase the statistics near $y = 0$.

would be just the calculation of an energy. Nevertheless, this approach allows us to treat nonequilibrium, nonstationary processes, such as fractional Brownian motion, within the same framework as conventional equilibrium statistical mechanics systems. Hence, the approach should be applicable to a wide range of problems.

III. RESULTS

We have performed simulations to generate fBm's for values of the Hurst exponent $H = 1/4$, $H = 2/5$, $H = 1/2$, $H = 2/3$, and $H = 3/4$ of lengths $L = 10^3$, 10^4, 10^5, 10^6, and 10^7, respectively (for $H = 3/4$ we did not consider $L = 10^5$ and $L = 10^6$ since this was not necessary). For the rescaling, we used $a = 2$ ($H = 1/4$), $a = 1.5$ ($H = 2/5$), $a = 1.2$ ($H = 1/2$), $a = 0.5$ ($H = 2/3$), and $a = 0.4$ ($H = 3/4$). In each case, we determined the parameter p such that the acceptance probability was (very roughly) 0.5. The values we used are shown in Table I. In each case the MC simulation was performed for long runs, up to $t = 3 \times 10^8$ for the longest walks of length $L = 10^7$.

Note that for $H = 1/4$, $H = 2/5$, and $H = 1/2$, we have restricted the simulations to fBm processes with $y > 0.0001$ to prevent the simulation from being caught near $y = 0$ due

TABLE I. Value of the Monte Carlo parameter p for different lengths of the fBm's and different values of the Hurst exponent H.

L	$H = 1/4$	$H = 2/5$	$H = 1/2$	$H = 2/3$	$H = 3/4$
10^3	0.010	0.060	0.030	0.40	0.50
10^4	0.020	0.020	0.020	0.40	0.50
10^5	0.020	0.030	0.020	0.20	
10^6	0.010	0.020	0.020	0.10	
10^7	0.015	0.020	0.015	0.05	0.05

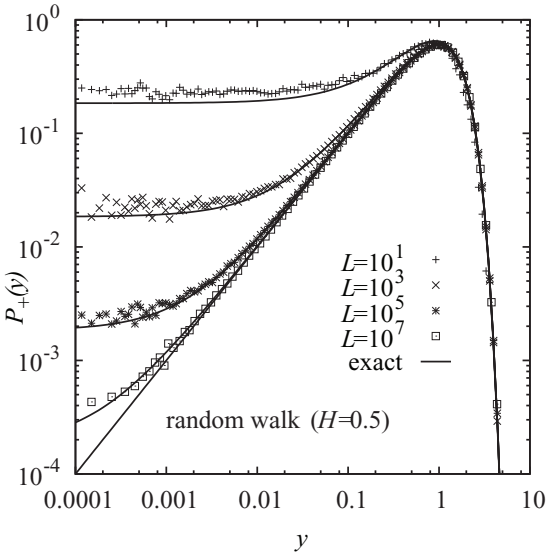

FIG. 3. Distribution $P_+(y)$ of the rescaled endpoints $y = x/L^H$ for nonabsorbed fBm's (Hurst exponent $H = 1/2$).

to a very small acceptance ratio via the rescaling factor in that region.

First, to verify our method, we studied the case of standard random walks, where $H = 1/2$. For this case the first corrections to the continuum limit behavior are known (see the Appendix):

$$P_+(y,L) = f_0(y) - \frac{c}{\sqrt{L}} f_1(y) + \cdots, \tag{9}$$

where L is the number of increments, and the constant c depends on the increments' distribution of the random walk. For Gaussian numbers (zero mean, unit variance) we have $c = \zeta(1/2)/\sqrt{2\pi} \sim -0.582\,597\ldots$ and the scaling functions are

$$f_0(y) = y\, e^{-y^2/2}, \qquad f_1(y) = \left(1 - \frac{2y}{\pi}\right) e^{-y^2/2}. \tag{10}$$

The rescaled distributions $P_+(y)$ of the endpoints are, together with the predictions of Eq. (9) valid for large L, shown in Fig. 3. One is able to see strong finite-size effects for small values $y \to 0$, where a plateau is visible. For increasing length L, the plateau decreases as $c/\sqrt{L}$ and the data increasingly approach the continuum limit scaling function f_0.

We conclude that for a generic fBm for which first corrections to the continuum limit behavior is not known, this plateau should also vanish when the size of the system is large. Indeed for very long walks ($L = 10^7$) the continuum limit behavior is observed over several orders of magnitude.

Based on scaling arguments it has been conjectured [7] that in the continuum limit $P_+(y)$ vanishes as y^ϕ with $\phi = (1 - H)/H = \theta/H$ for $y \to 0$, θ being the persistence defined via Eq. (8). This conjecture was confirmed by an epsilon expansion around the Brownian solution obtained by a field theory calculation [19]. A numerical check of the conjecture for values of H far from $1/2$ remains very challenging. We first consider the discrete random walk with $H = 2/3$. In this case, since the persistence is decreasing slowly ($\theta = 1/3$),

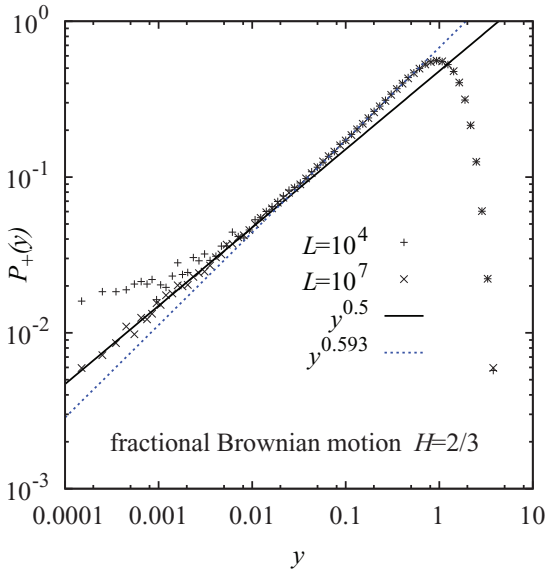

FIG. 4. (Color online) Distribution $P_+(y)$ of the rescaled endpoints $y = x/L^H$ for nonabsorbed fBm's (Hurst exponent $H = 2/3$).

numerical results were obtained for moderate lengths $L = 2 \times 10^4$ by direct simulations [19], which were compatible with the analytics. Here, we studied this case again. Our results, up to a length of $L = 10^7$, confirm the analytics with much better accuracy, as the small-endpoint behavior follows the expected power law with exponent $\phi = 1/2$ very well (see Fig. 4). For the case $H = 3/4$, the behavior close to the origin also matches the expected $P(y) \sim y^\phi$ behavior with $\phi = 1/3$ very well (see Fig. 5).

In the subdiffusive case, convergence with the increasing length L of the path is slower. We first consider the case $H = 2/5$ (see Fig. 6). For the longest walk, the behavior close to the origin follows a power law $P(y) \sim y^{\phi_{\rm eff}}$, but the exponent $\phi_{\rm eff} = 1.44(1)$ (obtained from fitting a power

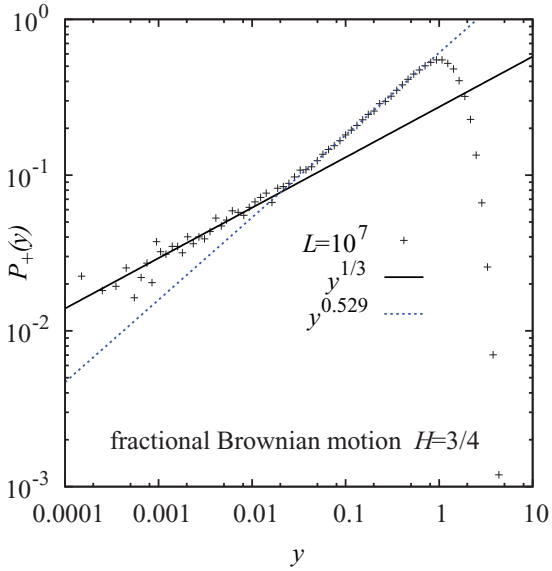

FIG. 5. (Color online) Distribution $P_+(y)$ of the rescaled endpoints $y = x/L^H$ for nonabsorbed fBm's (Hurst exponent $H = 3/4$).

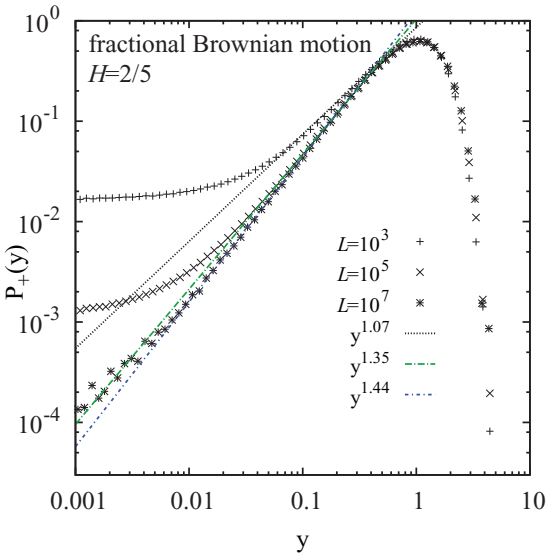

FIG. 6. (Color online) Distribution $P_+(y)$ of the rescaled endpoints $y = x/L^H$ for nonabsorbed fBm's (Hurst exponent $H = 2/5$).

law in the region $y \in [0.03,0.2]$) is slightly smaller than the predicted value $\phi = (1 - H)/H = 3/2$. A better estimation is obtained by performing a finite-length extrapolation of the form

$$\phi_{\rm eff}(L) = \phi + cL^{-b} \tag{11}$$

for the effective exponent as a function of the length L (Fig. 7). When fitting Eq. (11) to the data, we obtained $\phi = 1.50(4)$ [and $b = 0.23(4)$], which is in perfect agreement with the prediction.

Finally, we turn to the most difficult case with $H = 1/4$, where we expect that $P_+(y) \approx y^3$ near $y = 0$. Direct simulations of this process (for restricted sizes) are not conclusive

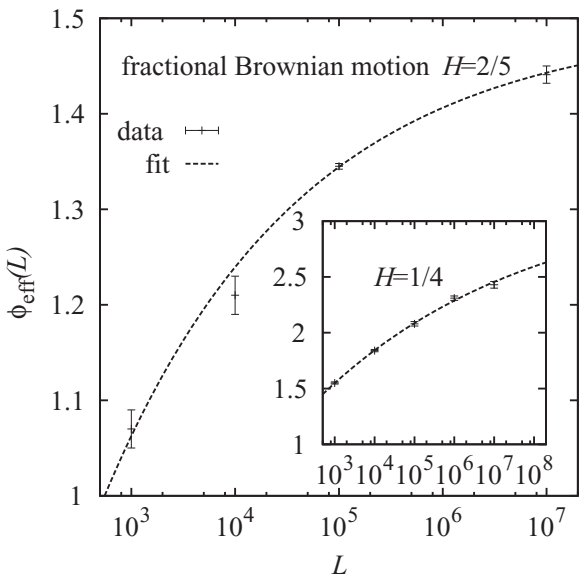

FIG. 7. Effective exponent $\phi_{\rm eff}$ as a function of the walk length L for $H = 2/5$. The line shows a fit to the function $\phi_{\rm eff}(L) = \phi + aL^{-b}$. Inset: for the case $H = 1/4$.

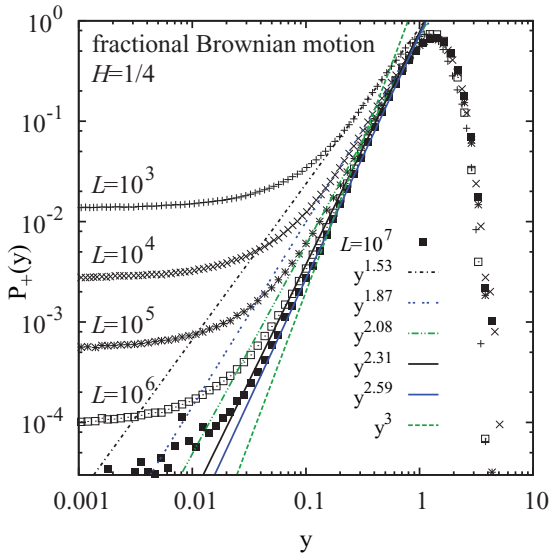

FIG. 8. (Color online) Distribution $P_+(y)$ of the rescaled endpoints $y = x/L^H$ for nonabsorbed fBm's (Hurst exponent $H = 1/4$).

and a scaling behavior $\sim y^2$ was found to be consistent with the data [27,32]. Using our Markov chain approach we can see the finite-size effects remain important even for long processes (see Fig. 8). Again, as in the case $H = 2/5$, we observed power law behavior close to the origin with an effective exponent $\phi_{\rm eff}(L)$. From $L = 10^5$ on, the effective exponent is above 2 and is growing with walk length L. Hence, the previous claim of quadratic behavior can be clearly discarded. Here the extrapolation according to Eq. (11) yields $\phi = 3.3(3)$ with a very slow convergence [$b = 0.08(2)$]. Hence, even if one was able to study extremely long walks like $L = 10^{11}$, one would observe $\phi_{\rm eff} \approx 2.88$. Thus, the observed extrapolated exponent is also compatible, within error bars, with the predicted value $\phi = 3$, but with lower accuracy due to stronger finite-length correction.

IV. SUMMARY

We have introduced a Markov chain Monte Carlo approach to study numerically fractional Brownian motion in the presence of an absorbing boundary via generating finite-step random walks with correlated disorder. Our approach allowed us to study walks of up to $L = 10^7$ steps. For the test case $H = 1/2$, the resulting distribution $P_+(y)$ of the rescaled endpoints y of the walks agrees in the limit $L \to \infty$ with the exact analytic result. We also derived analytical expressions for the finite-length corrections, which are also compatible with the numerical results, increasingly so with increasing step number L.

In the main part of our work, we studied fractional Brownian motion where we find for $y \to 0$ power law behaviors $P_+(y) \sim y^\phi$. For the superdiffusive cases, $H = 2/3$ and $H = 3/4$, we observed for long walks $L = 10^7$ that the measured exponents match the analytical prediction $\phi = (1 - H)/H$ with very good accuracy.

For the subdiffusives cases $H = 2/5$ and $H = 1/4$ we found strong finite-length effects which can be described via an effective exponent $\phi_{\rm eff}(L)$. Therefore, we could not observe the limiting exponent directly. However, in both cases we found via a power law extrapolation a convergence to the predicted values $\phi = (1 - H)/H$.

ACKNOWLEDGMENTS

We thank S. Franz for interesting discussions concerning the detailed balance of the approach, leading to the concise presentation given here. We thank C. Cook for critically reading the manuscript. A.K.H. acknowledges the hospitality of the Aspen Center for Physics, which is supported by National Science Foundation Grant No. PHY-1066293. The simulations were performed at the University of Oldenburg HERO high-performance computing facility which is funded by the DFG, INST 184/108-1 FUGG and the Ministry of Science and Culture (MWK) of the Lower Saxony state. A.K.H. thanks the Université Paris Sud and in particular Marc Mézard for their hospitality during several visits. S.N.M. would like to acknowledge support by ANR Grant No. 2011-BS04-013-02 WALKMAT. S.N.M and A.R. acknowledge support from the Indo-French Centre for the Promotion of Advanced Research under Project No. 4604-3.

APPENDIX: DERIVATION OF EQS. (8) AND (9)

We consider a random walk starting at the origin. Its position at discrete time steps evolves via

$$x_n = x_{n-1} + \eta_n \tag{A1}$$

starting from $x_0 = 0$. The random variables η_n are independent, identically distributed noises, each drawn from a symmetric and continuous probability density function (pdf) $f(\eta)$. Let $p_L(x)$ denote the probability density of the particle arriving at x at step L, while remaining positive during all intermediate steps. An exact expression for $p_L(x)$, or rather for its generating function, is known explicitly for arbitrary jump density $f(\eta)$ and is given by [33]

$$\int_0^\infty dx\, e^{-\lambda x} \sum_{L=0}^{\infty} p_L(x)\, s^L = \phi(s,\lambda) \tag{A2}$$

with

$$\varphi(s,\lambda) = \exp\left(-\frac{\lambda}{\pi}\int_0^\infty \frac{\ln[1 - s\,\hat{f}(k)]}{k^2 + \lambda^2}\, dk\right), \tag{A3}$$

where $\hat{f}(k) = \int_{-\infty}^{\infty} e^{i\,k\,\eta}\, f(\eta)\, d\eta$ is the Fourier transform of the noise density. Our goal is to extract the leading (and subleading) scaling behavior of $p_L(x)$ for large L from Eq. (A2).

As an intermediate step, it is useful to consider an alternative expression for $\phi(s,\lambda)$ derived in Ref. [34], valid for all $f(\eta)$'s with a finite variance $\sigma^2 = \int_{\infty}^{\infty} \eta^2\, f(\eta)\, d\eta$,

$$\phi(s,\lambda) = \frac{1}{[\sqrt{1-s} + \sigma\,\lambda\,\sqrt{s/2}]} \times \exp\left[-\frac{\lambda}{\pi}\int_0^\infty \frac{dk}{\lambda^2 + k^2} \ln\left(\frac{1 - s\,\hat{f}(k)}{1 - s + s\,\sigma^2 k^2/2}\right)\right]. \tag{A4}$$

We next consider the scaling limit when $x \to \infty$, $L \to \infty$, with the ratio $y = x/\sqrt{L}$ fixed. In the Laplace space, this corresponds to taking the limit $\lambda \to 0$, $s \to 1$, keeping the ratio $\lambda/\sqrt{1-s}$ fixed. Taking this scaling limit in Eq. (A4), one sees that

$$\phi(s,\lambda) \to \frac{1 - c\,\lambda}{\sqrt{1-s} + \sigma\,\lambda/\sqrt{2}}, \tag{A5}$$

where c is a constant and given by the following expression [34,35]:

$$c = \frac{1}{\pi} \int_0^\infty \frac{dk}{k^2} \ln\left[\frac{1 - \hat{f}(k)}{\sigma^2 k^2/2}\right]. \tag{A6}$$

Substituting the scaling-limit expression of $\phi(s,\lambda)$ from Eq. (A5) on the right hand side of Eq. (A2) and inverting the Laplace transform with respect to λ gives

$$\sum_{L=0}^{\infty} p_L(x)\, s^L \approx \frac{\sqrt{2}}{\sigma}\left[1 + \frac{\sqrt{2}}{\sigma}\, c\,\sqrt{1-s}\right] e^{-\sqrt{2\,(1-s)}\,x/\sigma}, \tag{A7}$$

which is valid in the scaling limit $s \to 1$, $x \to \infty$ while keeping the product $\sqrt{1-s}\,x$ fixed. Next, one can invert this generating function with respect to s using Cauchy's inversion formula. Skipping the details, we find that the two leading terms, in the scaling limit where $x \to \infty$, $L \to \infty$ while keeping $y = x/\sqrt{L}$ fixed, are given by

$$p_L(x) \approx \frac{1}{\sigma^2\sqrt{\pi}\,L}\left[y\, e^{-y^2/2\sigma^2} - \frac{c}{\sqrt{L}}\, e^{-y^2/2\sigma^2}\right]. \tag{A8}$$

The conditional probability $P_L(x)$ (probability density of reaching the position x given that it has survived L steps) is defined as

$$P_L(x) = \frac{p_L(x)}{\int_0^\infty p_L(x)\,dx}. \tag{A9}$$

Substituting the scaling behavior for $p_L(x)$ from Eq. (A8) in the above definition, we find that $P_L(x)$ has the following scaling behavior:

$$P_L(x) \to \frac{1}{\sqrt{L}}\, P_+(y,L) \tag{A10}$$

with $y = x/\sqrt{L}$ and

$$P_+(y,L) = f_0(y) - \frac{c}{\sqrt{L}}\, f_1(y) + O(1/L), \tag{A11}$$

where

$$f_0(y) = \frac{y}{\sigma^2}\, e^{-y^2/2\sigma^2}, \tag{A12}$$

$$f_1(y) = e^{-y^2/2\sigma^2} - \frac{2}{\pi\sigma}\, y\, e^{-y^2/2\sigma^2}, \tag{A13}$$

and c as defined by Eq. (A6). For the special case of the Gaussian jump density, $f(\eta) = e^{-\eta^2/2}/\sqrt{2\pi}$ (with $\sigma^2 = 1$), one can evaluate the constant c in Eq. (A6) explicitly [34],

$$c = \frac{\zeta(1/2)}{\sqrt{2\pi}} = -0.582\,597\ldots. \tag{A14}$$

In this case, setting $y = 0$ we get

$$P_+(0,L) \approx -\frac{c}{\sqrt{L}} = \frac{0.582\,597\ldots}{\sqrt{L}}, \tag{A15}$$

which is consistent with our simulations.

[1] B. B. Mandelbrot and J. W. van Ness, SIAM Rev. **10**, 422 (1968).

[2] Y. Kantor and M. Kardar, Phys. Rev. E **69**, 021806 (2004).

[3] J. Krug, H. Kallabis, S. N. Majumdar, S. J. Cornell, A. J. Bray, and C. Sire, Phys. Rev. E **56**, 2702 (1997).

[4] T. E. Harris, J. Appl. Probab. **2**, 323 (1965).

[5] S. N. Majumdar and M. Barma, Phys. Rev. B **44**, 5306 (1991).

[6] J.-C. Walter, A. Ferrantini, E. Carlon, and C. Vanderzande, Phys. Rev. E **85**, 031120 (2012).

[7] A. Zoia, A. Rosso, and S. N. Majumdar, Phys. Rev. Lett. **102**, 120602 (2009).

[8] D. Panja and G. T. Barkema, J. Chem. Phys. **132**, 014902 (2010).

[9] D. Panja, G. T. Barkema, and R. C. Ball, J. Phys.: Condens. Matter **19**, 432202 (2007).

[10] J. Szymanski and M. Weiss, Phys. Rev. Lett. **103**, 038102 (2009).

[11] S. C. Weber, A. J. Spakowitz, and J. A. Theriot, Phys. Rev. Lett. **104**, 238102 (2010).

[12] J. H. Jeon, H. Martinez-Seara Monne, M. Javanainen, and R. Metzler, Phys. Rev. Lett. **109**, 188103 (2012).

[13] L. Lizana, T. Ambjörnsson, A. Taloni, E. Barkai, and M. A. Lomholt, Phys. Rev. E **81**, 051118 (2010).

[14] R. García-García, A. Rosso, and G. Schehr, Phys. Rev. E **81**, 010102 (2010).

[15] G. Oshanin, A. Rosso, and G. Schehr, Phys. Rev. Lett. **110**, 100602 (2013).

[16] R. Cakir, P. Grigolini, and A. A. Krokhin, Phys. Rev. E **74**, 021108 (2006).

[17] I. Goychuk, Phys. Rev. E **80**, 046125 (2009).

[18] J.-H. Jeon and R. Metzler, Phys. Rev. E **81**, 021103 (2010).

[19] K. J. Wiese, S. N. Majumdar, and A. Rosso, Phys. Rev. E **83**, 061141 (2011).

[20] Better results for direct sampling can be obtained by making use of the fact that for fBm the matrix C is also a Toeplitz matrix. For Toeplitz matrices efficient numerical methods allow us to avoid the full diagonalization of C. An example is given by the Levinson algorithm (for a practical implementation of Levinson's algorithm, see T. Dieker, http://www2.isye.gatech.edu/~adieker3/fbm/index.html). However here we use a Markov chain sampling (not compatible with the Levinson algorithm) which is more efficient in the presence of absorption.

[21] A. T. A. Wood and G. Chan, J. Comput. Graph. Stat. **3**, 409 (1994).

[22] C. R. Dietrich and G. N. Newsam, SIAM J. Sci. Comput. **18**, 1088 (1997).

[23] L. E. Wittig and A. K. Sinha, J. Acoust. Soc. Am. **58**, 630 (1975).
[24] M. Galassi, J. Davies, J. Theiler, B. Gough, G. Jungman, M. Booth, and F. Rossi, *GNU Scientific Library Reference Manual* (Network Theory Ltd., Bristol, UK, 2006).
[25] S. N. Majumdar, Curr. Sci. **77**, 370 (1999).
[26] A. J. Bray, S. N. Majumdar, and G. Schehr, Adv. Phys. **62**, 225 (2013).
[27] A. Amitai, Y. Kantor, and M. Kardar, Phys. Rev. E **81**, 011107 (2010).
[28] A. K. Hartmann, Phys. Rev. E **65**, 056102 (2002).
[29] A. Engel, R. Monasson, and A. K. Hartmann, J. Stat. Phys. **117**, 387 (2004).
[30] A. K. Hartmann, Eur. Phys. J. B **84**, 627 (2011).
[31] A. K. Hartmann, *Practical Guide to Computer Simulations* (World Scientific, Singapore, 2009).
[32] Y. Kantor and M. Kardar, Phys. Rev. E **76**, 061121 (2007).
[33] V. V. Ivanov, Astron. Astrophys. **286**, 328 (1994).
[34] A. Comtet and S. N. Majumdar, J. Stat. Mech.: Theory Exp. (2005) P06013.
[35] S. N. Majumdar, A. Comtet, and R. M. Ziff, J. Stat. Phys. **122**, 833 (2006).